Supporting Information

Single Metal Site and Versatile Transfer Channel Merged into Covalent Organic Frameworks Facilitate High-Performance Li-CO_2 Batteries

Yu Zhang,[†,⊥] Rong-Lin Zhong,[#,⊥] Meng Lu,[†,⊥] Jian-Hui Wang,[†] Cheng-Jiang,[†] Guang-Kuo Gao,[†] Long-Zhang Dong,[†] Yifa Chen,[†] Shun-Li Li[†] and Ya-Qian Lan*[,†,‡]

[†] Jiangsu Collaborative Innovation Centre of Biomedical Functional Materials, Jiangsu Key Laboratory of New Power Batteries, School of Chemistry and Materials Science, Nanjing Normal University, Nanjing 210023, P. R. China.

[‡] School of Chemistry, South China Normal University, Guangzhou, 510006, P. R. China.

Laboratory of Theoretical and Computational Chemistry, Institute of Theoretical Chemistry, College of Chemistry, Jilin University, Changchun 130023, P. R. China.

[⊥] Yu-Zhang, Rong-Lin Zhong and Meng Lu contributed equally to this work.

Contents

Materials

All solvents and reagents obtained from commercial sources were used without further purification. Tetrathiafulvalene (≥98%, TTF) was purchased from Accela ChemBio Co., Ltd. Mesitylene (≥99.5%) was purchased from Sinopharm Chemical Reagent Co., Ltd and 1, 4-Dioxane (≥ 99.7%) from MACKLIN reagent. TAPP-2H was purchased from Kaiyulin (Shanghai) Development Co., Ltd. 4-Bromobenzaldehyde was purchased from Meryer (Shanghai) Chemical Technology Co., Ltd. $CHCl_3$ and Na_2SO_4 were purchased from Sinopharm Chemical Reagent Co., Ltd.

Synthesis Methods

Synthesis of 2,3,6,7-tetra (4-formylphenyl) tetrathiafulvalene (TTF-4CHO). The synthesis of 4-formyl-TTF has been reported.[1,2] Typically, TTF (1.0 g), 4-bromobenzaldehyde (4.5 g), $Pd(OAc)_2$ (0.28 g), $PtBu_3HBF_4$ (1.0 g), and Cs_2CO_3 (5.9 g) were put into a three-neck round-bottomed flask. After degassed and purification with high-purity nitrogen gas for three times, anhydrous tetrahydrofuran (THF) (50 mL) was added into the flask under nitrogen atmosphere. Then, the flask was heated at 75 °C with reflux and kept stirring for 30 h. After cooling to room temperature, the organic compounds were collected and extracted with $CHCl_3$ (100 mL) for three times followed with vacuum filtration to remove the undissolved solid. Then, the obtained organic phase was washed with brine (100 mL) for several times by using a pear-shaped separatory funnel and was dried with anhydrous Na_2SO_4. After that, the organic phase was collected to afford crude product (dark red) through rotary evaporation to remove the solvent. The resulted sample was purified by column chromatography with silica using dichloromethane : acetone = 500 : 3 as mobile phase to achieve pure product 4-formyl-TTF (0.9 g) (red, ~30% yield).

Synthesis of 5,10,15,20-tetrakis (para-aminophenyl) porphyrin manganese (II) (TAPP-Mn). The synthesis method of TAPP-Mn follows previously reported procedures with modified.[3] In detail, $Mn(OAc)_2 \cdot 2H_2O$ (1.2 mmol) and TAPP-2H (0.3 mmol) were added in a three-neck round-bottomed flask. After purification with high-purity nitrogen gas, a mixed solvent of methanol (20 mL), chloroform (90 mL), and N,N'-dimethylformamide (30 mL) were added. The flask was heated at 80 °C with stirring under nitrogen atmosphere for 24 h. After cooling to room temperature, the solution was transferred into a separatory funnel and washed with water. After that, the solution was collected through rotary evaporation to obtain dark purple solid (TAPP-Mn, ~180 mg, ~85% yield).

Synthesis of TTCOF-Mn. The synthesis of TTCOF-Mn follows previously reported method.[4,5] A Pyrex tube measuring 19 × 65 mm (o.d × length) was charged with TAPP-Mn (15 mg, 0.02 mmol), TTF-4CHO (12.4 mg, 0.02 mmol), 1,4-dioxane (0.5 mL), 1,3,5-trimethylbenzene (0.5 mL) with ultrasonic for ~5 min to dissolve, then 6 M aqueous acetic acid (0.2 mL) were added. After sonication for another 15 minutes, the tube was flash frozen at 77 K (liquid N_2 bath) and degassed by three freeze-pump-thaw cycles and evacuated to an internal pressure of ~100 mTorr and sealed. After warmed to room temperature, the mixture was heated at 120 °C and left undisturbed for 72 hours. A dark purple precipitate was isolated by filtration in Buchner funnel and was washed

with THF and acetone until the filtrate was colorless. The wet sample was transferred to a Soxhlet extractor and washed with THF (24 hours) and acetone (24 hours). Finally, the product was evacuated at 150 °C under dynamic vacuum overnight to yield activated sample.

Synthesis of TTCOF-2H/Ni/Cu/Co. The synthesis of TTCOF-2H/Ni/Cu/Co was carried out following the same protocol as for TTCOF-Mn, by replacing the TAPP-Mn with TAPP-2H (13.5 mg, 0.02 mmol), TAPP-Ni (14.7 mg, 0.02 mmol), TAPP-Cu (14.8 mg, 0.02 mmol), and TAPP-Co (14.7 mg, 0.02 mmol).

Synthesis of COF-366-Mn. The synthesis of COF-366-Mn follows previously reported method.[31] A Pyrex tube measuring 19 × 65 mm (o.d × length) was charged with TAPP-Mn (13.5 mg, 0.018 mmol), BDA (5.6 mg, 0.042 mmol), ethanol (0.5 mL), 1,3,5-trimethylbenzene (0.5 mL), and ultrasonic for ~5 min to dissolve, then 6 M aqueous acetic acid (0.1 mL) were added. The remaining synthesis procedures are the same as TTCOF-Mn.

Characterizations and instruments

PXRD patterns were recorded on a D/max 2500VL/PC diffractometer (Japan) equipped with a graphite monochromatized Cu Kα radiation source (λ = 1.54060 Å). The corresponding working voltage and current are 40 kV and 150 mA, respectively. TEM and HR-TEM images were recorded on JEOL-2100F apparatus at an accelerating voltage of 200 kV. Morphological and microstructural analyses were conducted using a SEM (JSM-7600F) at an accelerating voltage of 10 kV. EDS was performed with a JSM-5160LV-Vantage type energy spectrometer. Nitrogen adsorption-desorption isotherms were recorded at 77 K using a Quantachrome instrument (Quantachrome Instruments Autosorb IQ2). The pore size distribution was calculated by nonlocal density functional theory (NLDFT). Fourier-transform infrared (FTIR) spectra of starting materials and COF samples were recorded in a Thermo Nicolet IS5 FTIR spectrometer under ambition conditions. Thermogravimetric analysis of COFs powder samples was performed on a Diamond TG/DTA/DSC Thermal Analyzer System (Perkin-Elmer, USA) with heating rate of 10 °C min^{-1} to 800 °C under air atmosphere. XPS was performed on a scanning X-ray microprobe (PHI 5000 Verasa, ULAC-PHI, Inc.) using Al Kα radiation and the C 1s peak at 284.6 eV as the internal standard. ICP-OES (Leeman Labs) was used to measure the content of metal ions. The I-V profiles tests were conducted with a probe station at room temperature (25 °C) under ambient conditions with a computer-controlled analog-to-digital converter (2636B, Kethley). The conductive sample was pressed into a sheet using a ton of pressure in the mold and the test voltage was among the range from -200 to 300 mV. The *in-situ* differential electrochemical mass spectrometry (DEMS) was performed using a commercial quadrupole mass spectrometer (Pfeiffer Vacuum, ThermoStar) and a customized Swagelok-type DEMS cell. The DEMS system was purged with 1.2 mL/min pure Ar for 10 h before charge and the current density of charge reaction during DEMS tests is 500 mA/g. The *ex-situ* examination of the gas products during discharge process of different TTCOF-M cathode catalysts were measured using gas chromatography (GC-7920A, Aulight Co., China) with an FID detector to analyze air/CO/CO_2.

Electrochemical Measurements

The electrochemical performance of Li-CO_2 batteries was tested using 2032 coin-type cells with the holes on the cathode side. The cells were composed of a lithium metal tablet anode, one slice of glass microfiber separator (Whatman), 0.2 mL of electrolyte, and a carbon paper coated with cathode material as the cathode (12 mm diameter). The batteries were assembled in an argon-filled glovebox and then installed in a home-made chamber. Before the measurements, the chambers were flushed with pure CO_2. Each measurement was begun after a 12 h open circuit potential step to ensure the equilibrium in the cell. The electrochemical measurements were carried out using a LAND cycler (CT2001A) and an electrochemical workstation (CHI660E; Shanghai Chenhua).

A mixture containing 70 wt% of cathode material, 20 wt% of KB as the conductive agent and 10 wt% of polyvinylidene fluoride as the binder was well mixed in N-methylpyrrolidone solvent by grinding. The as-obtained suspension was then dropped onto carbon paper, which served as a current collector. The cathodes were dried at 110 °C under vacuum for 12 h before use. The active material is both cathode material and KB. The mass loading of the active material (KB + catalyst) was controlled to be approximately 0.1-0.13 mg cm^{-2}, with the gravimetric current density and capacity normalized to the total cathode material. 1 M lithium bis(trifluoromethanesulfonyl) imide (LiTFSI) dissolved in tetraethylene glycol dimethyl ether was employed as the electrolyte, which was prepared in an argon-filled glovebox with water and oxygen contents below 0.1 ppm.

Calculation Setup

All geometry optimizations were performed by the m06 functional in gas phase. For the basis set, the Stuttgart-Dresden-Bonn basis sets were employed for valence electrons of transition metal atoms with effective core potentials representing their core electrons and 6-31G(d) basis sets were used for other atoms.[6,7] In addition, frequency calculations were conducted at the same theoretical level to verify whether it is a saddle point or minimum to obtain the thermodynamic properties at 298.15 K and 1 atm. To evaluate better potential energy, we performed single-point calculation by employing 6-311+G(d, p) basis sets for other atoms. All these calculations were carried out with Gaussian09 program.[8]

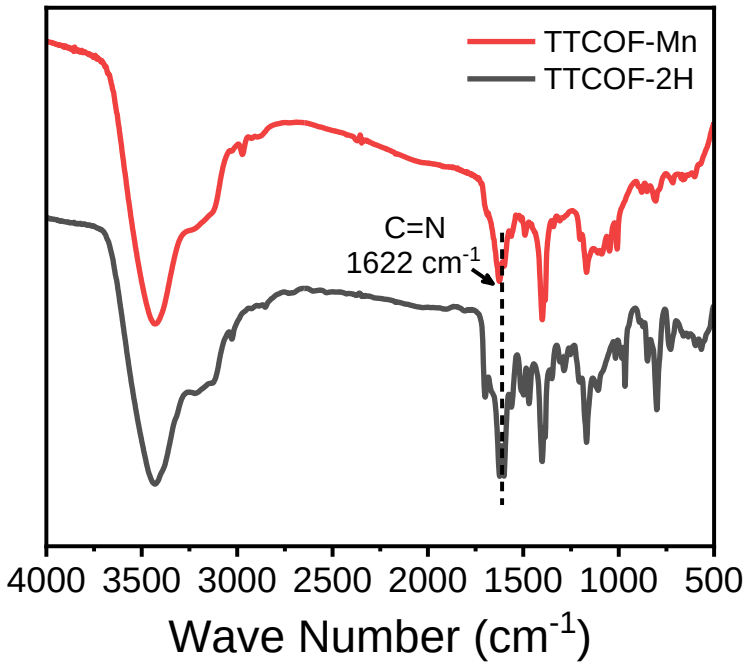

Figure S1. FTIR spectra of TTCOF-Mn and TTCOF-2H**.**

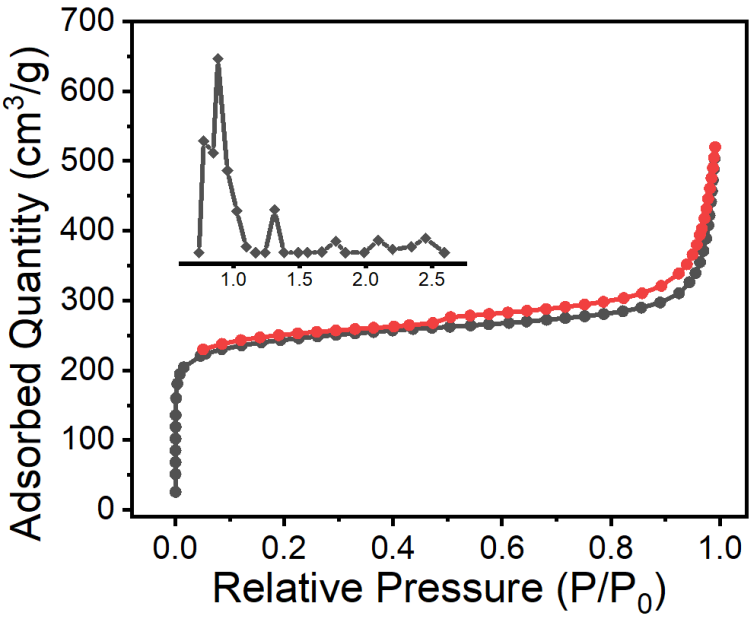

Figure S2. N_2 adsorption-desorption isotherms of TTCOF-Mn and the inset shows the pore width distribution.

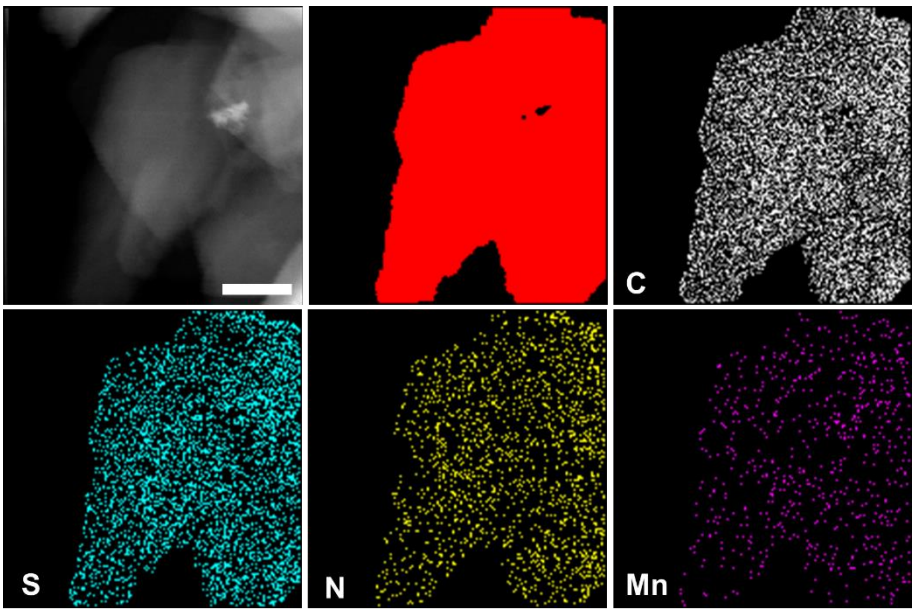

Figure S3. Energy-dispersive X-ray spectroscopy elemental mapping images of TTCOF-Mn (the second red image is the selected area), scale bar = 100 nm.

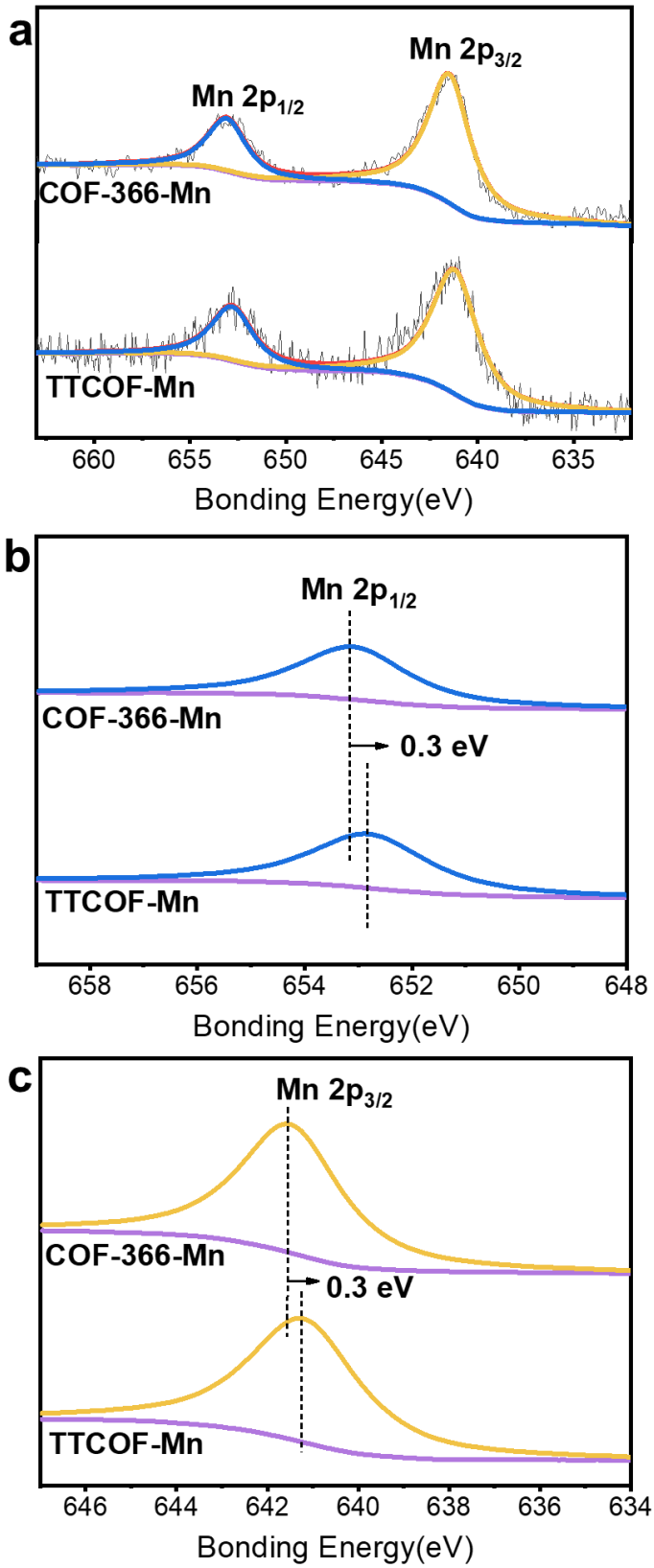

Figure S4. Mn 2p XPS spectra analysis of TTCOF-Mn and COF-366-Mn. (a) Mn 2p narrow scan, and enlarged view of (b) Mn $2p_{1/2}$ and (c) Mn $2p_{3/2}$.

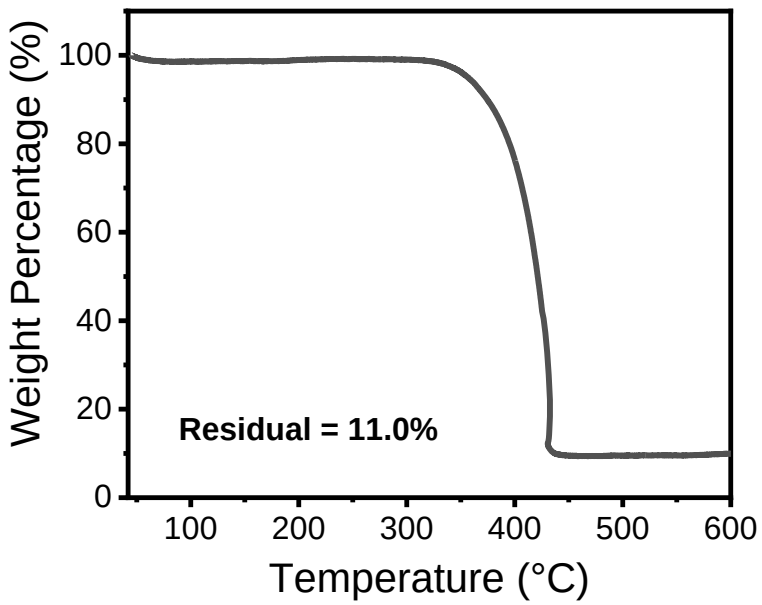

Figure S5. TGA curve of TTCOF-Mn in air atmosphere.

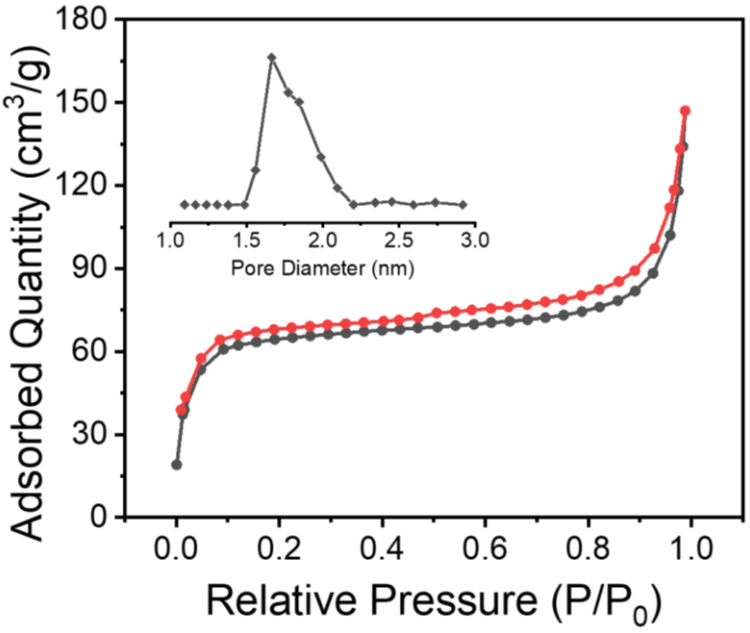

Figure S6. The N_2 adsorption-desorption isotherm and pore size distribution of COE-366-Mn.

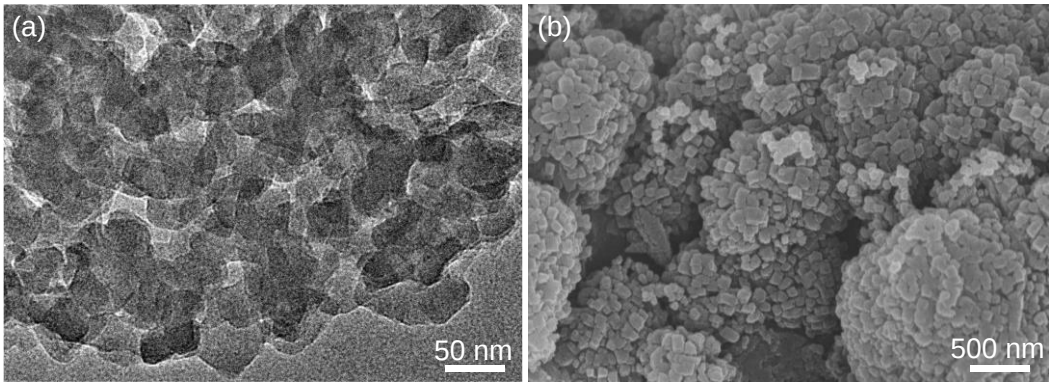

Figure S7. (a) TEM image and (b) SEM image of COE-366-Mn.

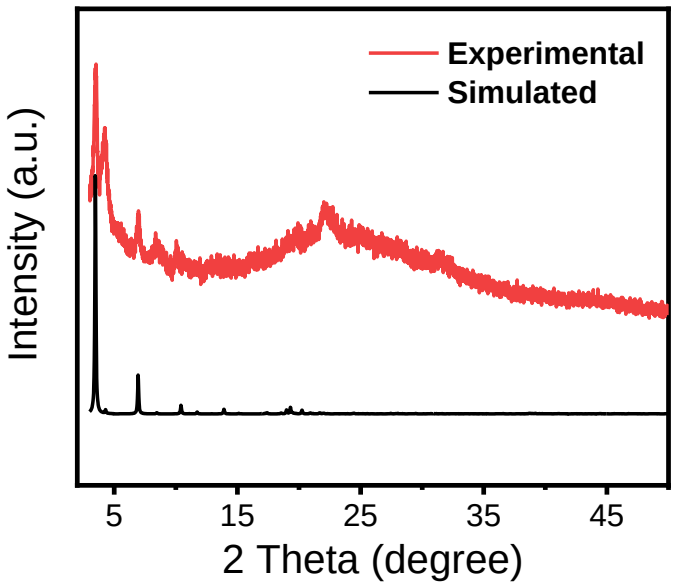

Figure S8. Experimental and simulated XRD patterns of COF-366-Mn.

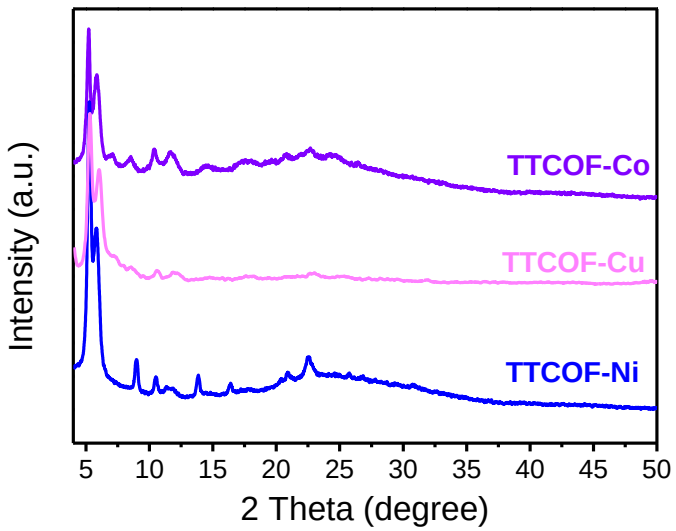

Figure S9. The XRD patterns of TTCOF- Co, TTCOF-Cu, and TTCOF-Ni.

Inductively coupled plasma atomic emission spectrometry (ICP) was used to determine the content of metal element measured on an ICP Atomic Emission Spectrometer (Prodigy, USA). Notes: Content %= m(Mn) / m (TTCOF-Mn) ×100 %

Table S1 ICP-AES test results of TTCOF-Mn.

Sample	Cal. (wt.%)	Found (wt.%)
TTCOF-Mn	4.31	4.11

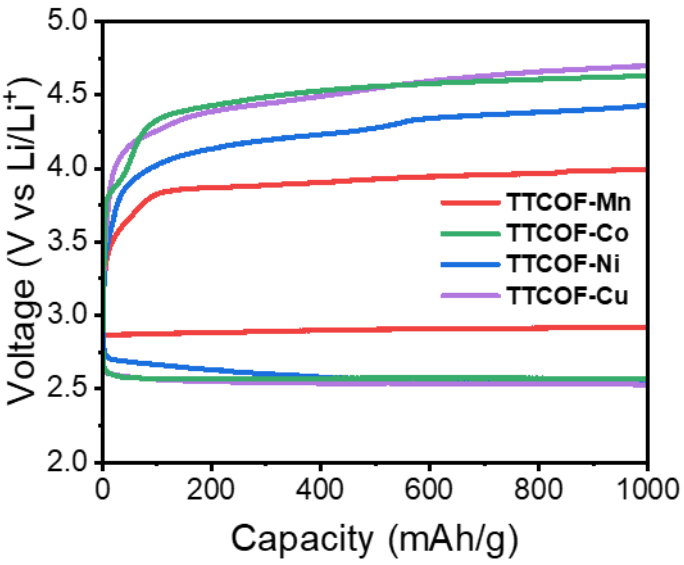

Figure S10. The discharge-charge curves of Li-CO_2 batteries with TTCOF-M (M = Mn, Co, Ni, Cu) cathodes at a current density of 100 mA/g with fixed capacity of 1000 mAh/g.

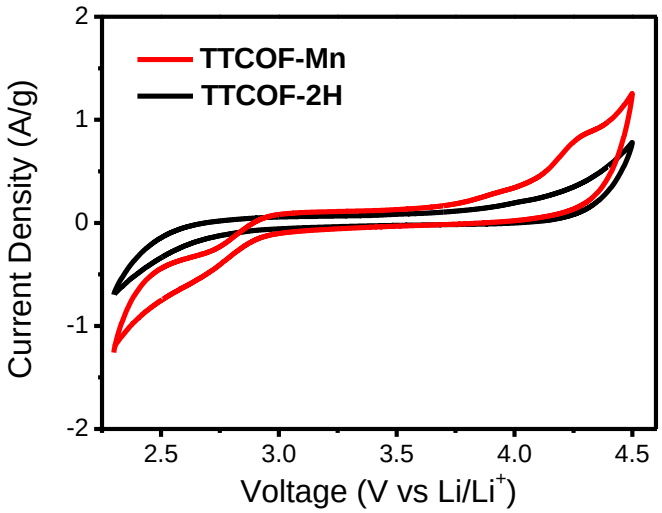

Figure S11. CV curves of the Li-CO_2 batteries with TTCOF-Mn cathode and TTCOF-2H cathode at 1 mV/s under CO_2 atmosphere.

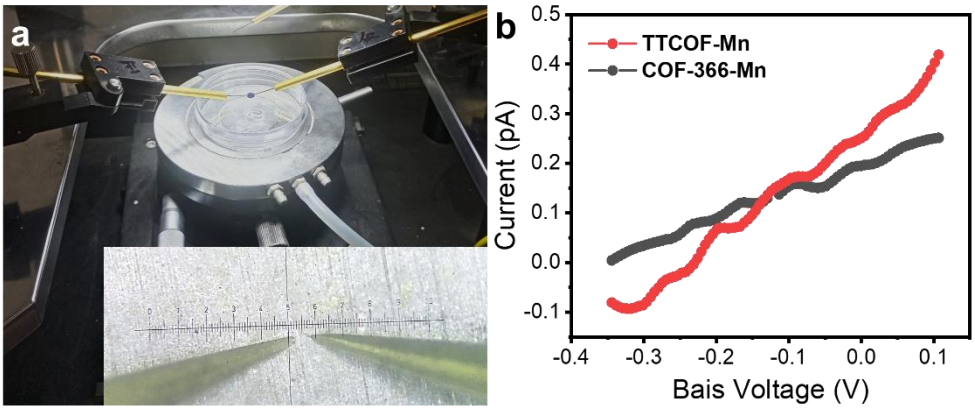

Figure S12. *I-V* profile tests and instrument. (a) The picture of the test instrument. (b) *I-V* curves of TTCOF-Mn and COF-366-Mn.

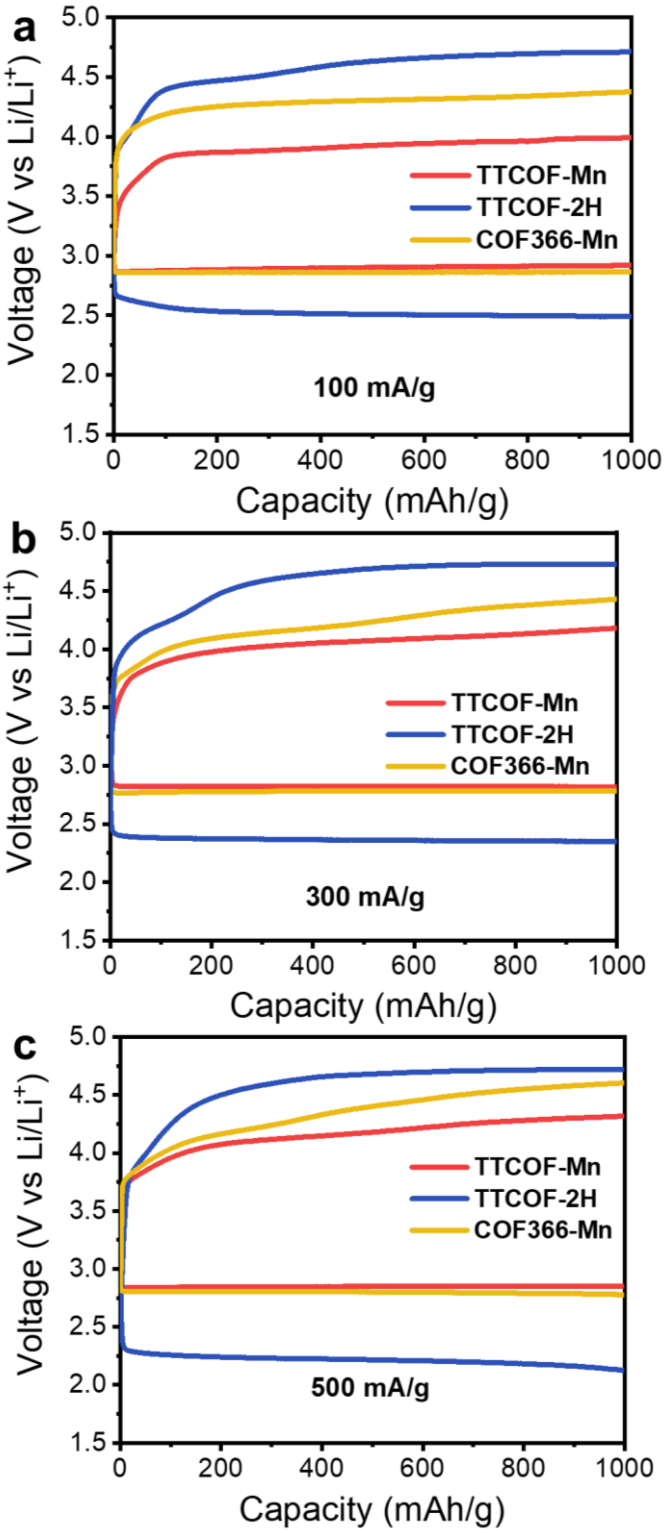

Figure S13. Discharge-recharge curves of TTCOF-Mn, TTCOF-2H, and COF366-Mn cathodes at different current densities of (a) 100 mA/g, (b) 300 mA/g, and (c) 500 mA/g.

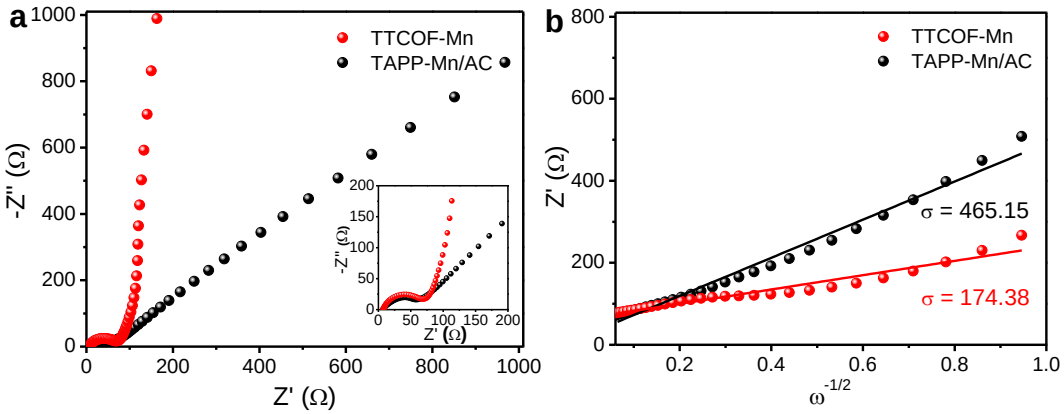

Figure S14. (a) Electrochemical impedance spectroscopy (EIS) of TTCOF-Mn and TAPP-Mn/AC cathodes. (b) Diffusion coefficients derived from the EIS.

The diffusion coefficient can be calculated according to the formula below.

$$D = \frac{R^2T^2}{A^2n^4F^4C^2\sigma^2} \qquad \textbf{(Equation S1)}$$

Where *R* is the gas constant, *T* is the absolute temperature, *A* is the surface area of the electrode, *n* is the number of electrons per molecule during oxidization, *F* is Faraday's constant, *C* is the concentration of Lithium ions, and σ is the Warburg factor (the slope value in **Figure S14b**).

The value of σ is negatively correlated to Li^+ transfer rate in the battery.[9] Therefore, the Li^+ transfer is faster in TTCOF-Mn than TAPP-Mn/AC cathode catalysts.

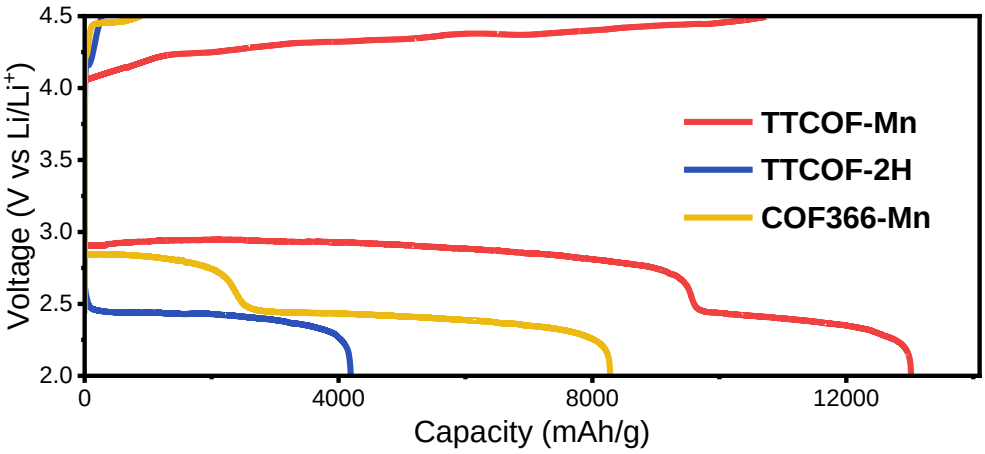

Figure S15. Deep discharge-recharge curves of TTCOF-Mn, TTCOF-2H and COF-366-Mn cathodes.

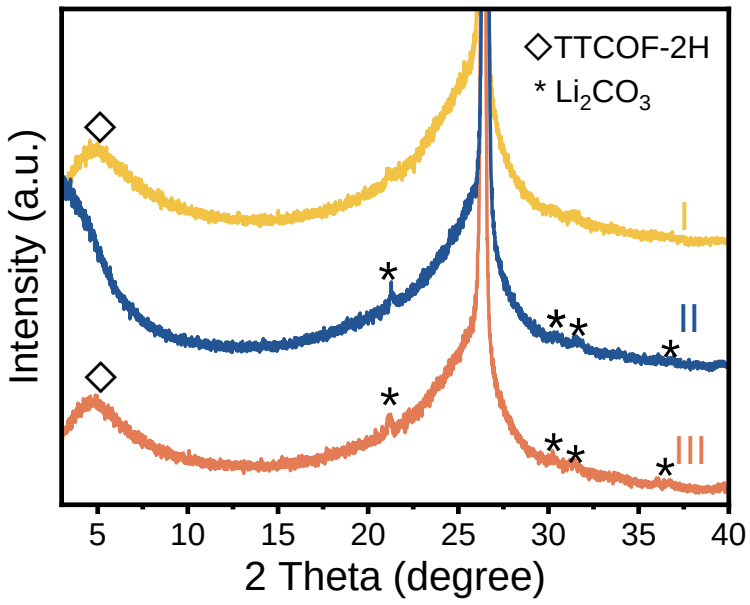

Figure S16. XRD patterns of TTCOF-2H cathodes at different stages in **Figure 3a**.

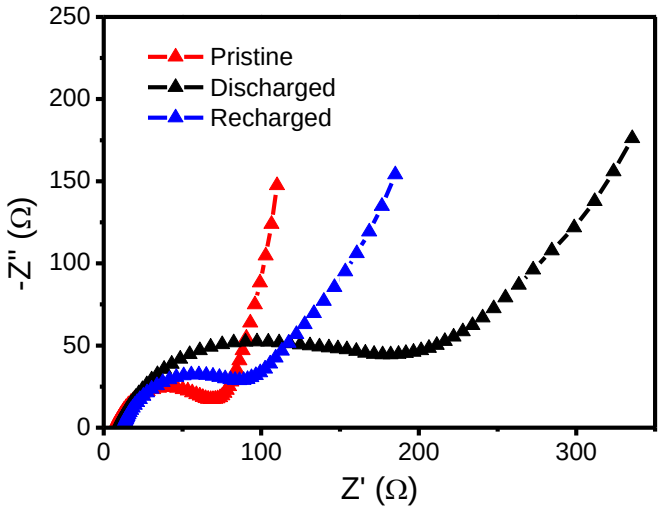

Figure S17. Impedance spectra of the Li-CO_2 battery with Mn-TTCOF cathode at pristine, discharged to 1000 mAh/g, and recharged back states.

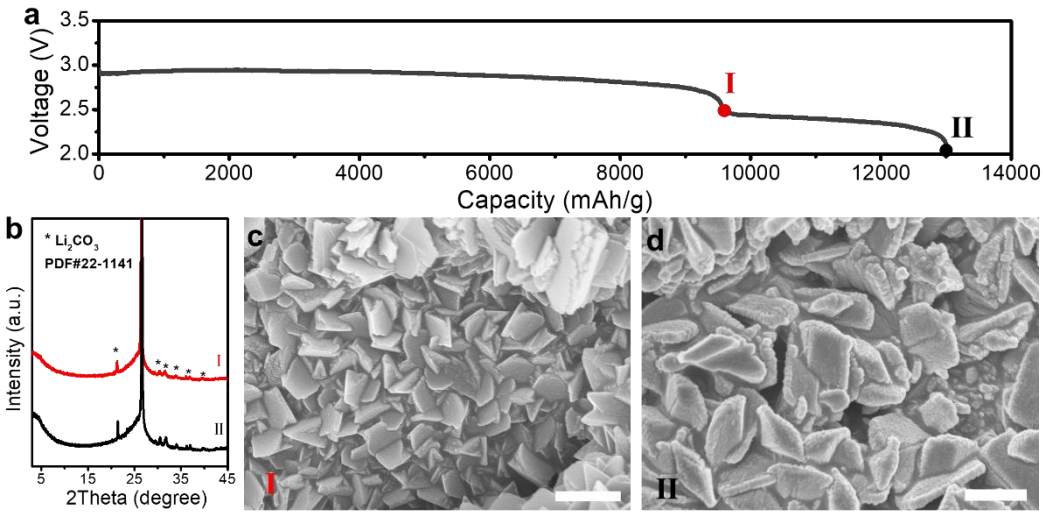

Figure S18. (a) First deep discharge curve of TTCOF-Mn cathode, (b) XRD patterns of TTCOF-Mn cathode at different stages in the first deep discharge curve: discharge to the end of the 1st plateau (*I*) and discharge to 2.0 V (*vs* Li/Li^+) (*II*). (c, d) SEM images observed of different stages in the first deep discharge process. Scale bar: 1 μm.

The products of battery with TTCOF-Mn after deep discharging have been characterized as well. As shown in **Figure S18**, there are two obvious plateaus in the deep discharge curve of TTCOF-Mn cathode. We detected the discharge products of at the end of both plateaus. It could be obtained that the products during discharging process are all crystalline Li_2CO_3 according to the XRD patterns in **Figure S18b**. And the generated Li_2CO_3 is rectangular slice with a width of approximately 500 nm for stage □ of the deep discharge process (**Figure S18c**). The Li_2CO_3 obtained at the end of second plateau are thicker and denser than those of the first plateau (**Figure S18d**). It could be deduced that TTCOF-Mn catalysts are active to CO_2 reduction during the initial discharging process and therefore the first plateau at ~2.9 V appears. And the continuous precipitation of Li_2CO_3 with a gradually increasing size would tightly cover the TTCOF-Mn catalyst, making the battery inactive, and thus the second plateau at ~2.5 V appears.

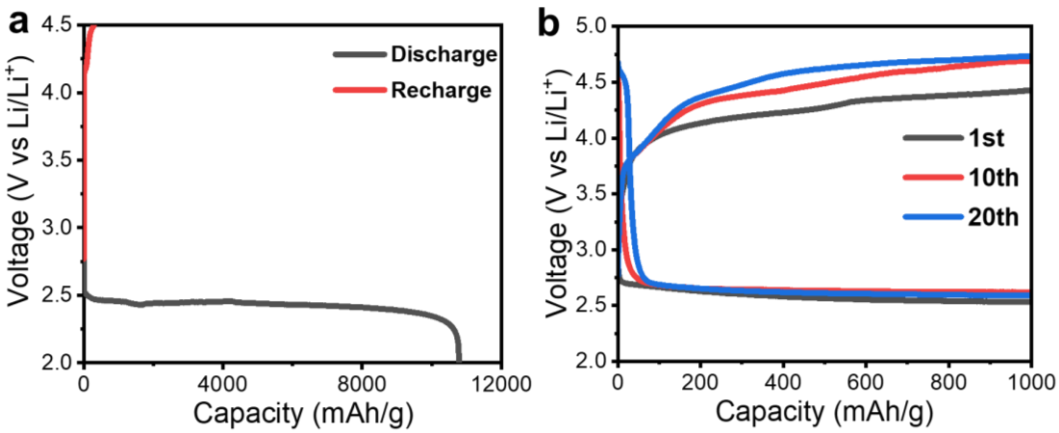

Figure S19. Electrochemical performance of Li-CO_2 battery using TTCOF-Ni. (a) Deep discharge-recharge curves and (b) Cycling performance at 100 mA/g.

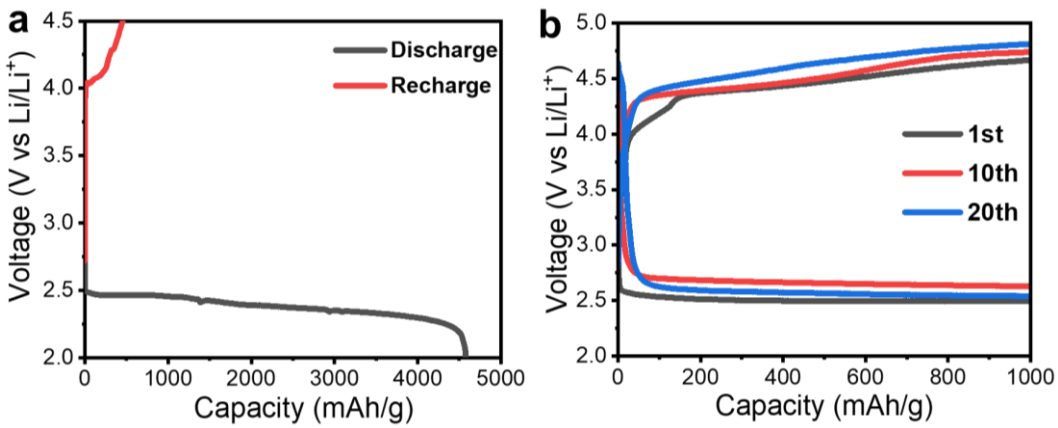

Figure S20. Electrochemical performance of Li-CO_2 battery using TTCOF-Cu. (a) Deep discharge-recharge curves and (b) Cycling performance at 100 mA/g.

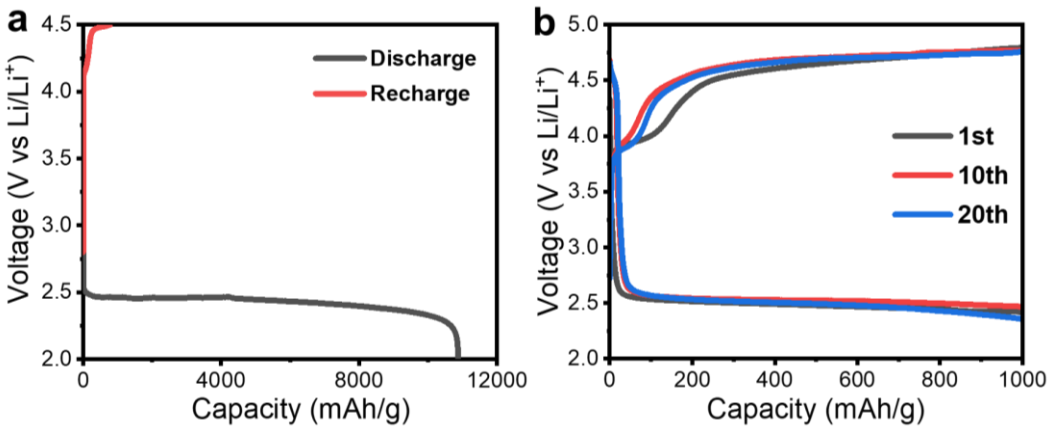

Figure S21. Electrochemical performance of Li-CO_2 battery using TTCOF-Co cathode. (a) Deep discharge-recharge curves and (b) Cycling performance at 100 mA/g.

S4 Mechanism of CO_2 conversion route with TTCOF-M cathodes

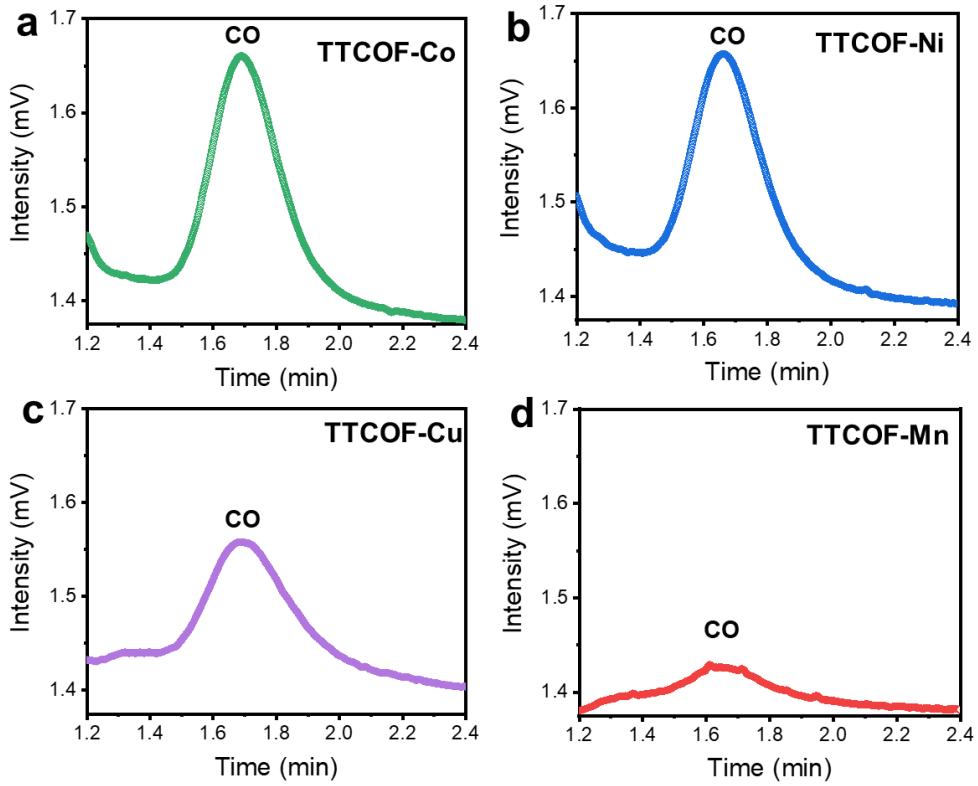

Figure S22. The gas chromatography (GC) analysis of discharge gas products of TTCOF-M cathodes.

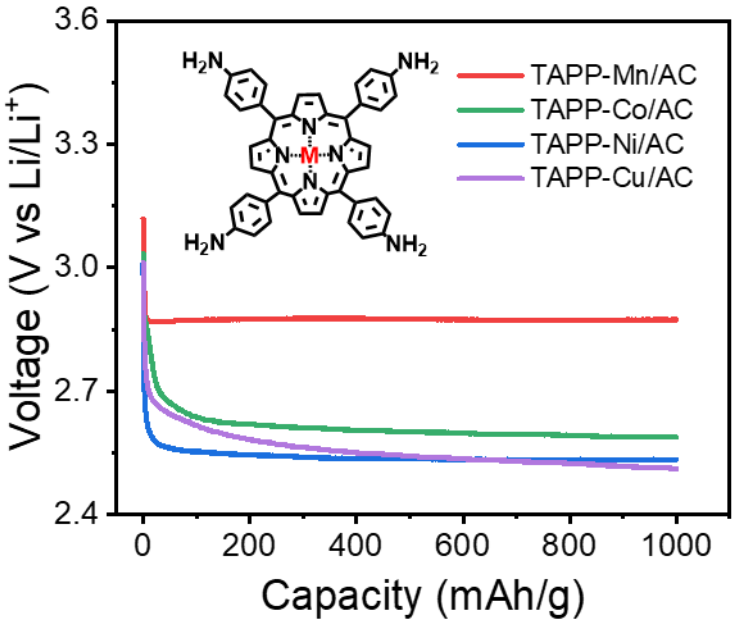

Figure S23. Discharging curves of Li-CO_2 batteries with TAPP-M/activated carbon (AC) cathodes (M = Mn, Co, Ni, Cu). The inset is the is the molecular formula of TAPP-M.

The TAPP-M performs similarly to the relevant TTCOF-M during discharge process. The discharge reaction plateau of TAPP-Mn/AC cathode is ~2.87 V and the other three TAPP-M/AC cathodes (M = Co, Ni, Cu) show similar discharge reaction plateaus from 2.47~2.56 V as shown in **Figure S23**.

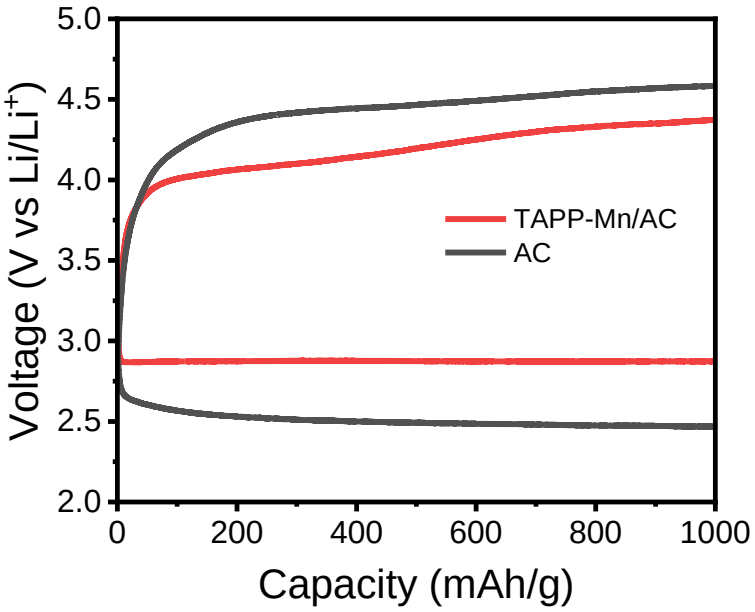

Figure S24. Discharging-charging curves of Li-CO_2 batteries with TAPP-Mn/activated carbon (AC) and activated carbon (AC) cathodes.

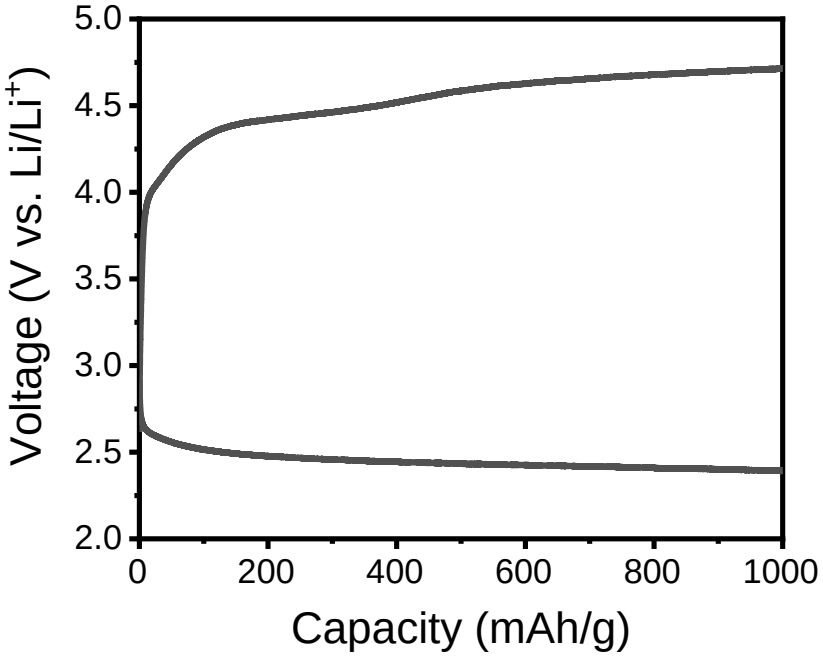

Figure S25. Discharging-charging curves of Li-CO_2 batteries with KB cathodes.

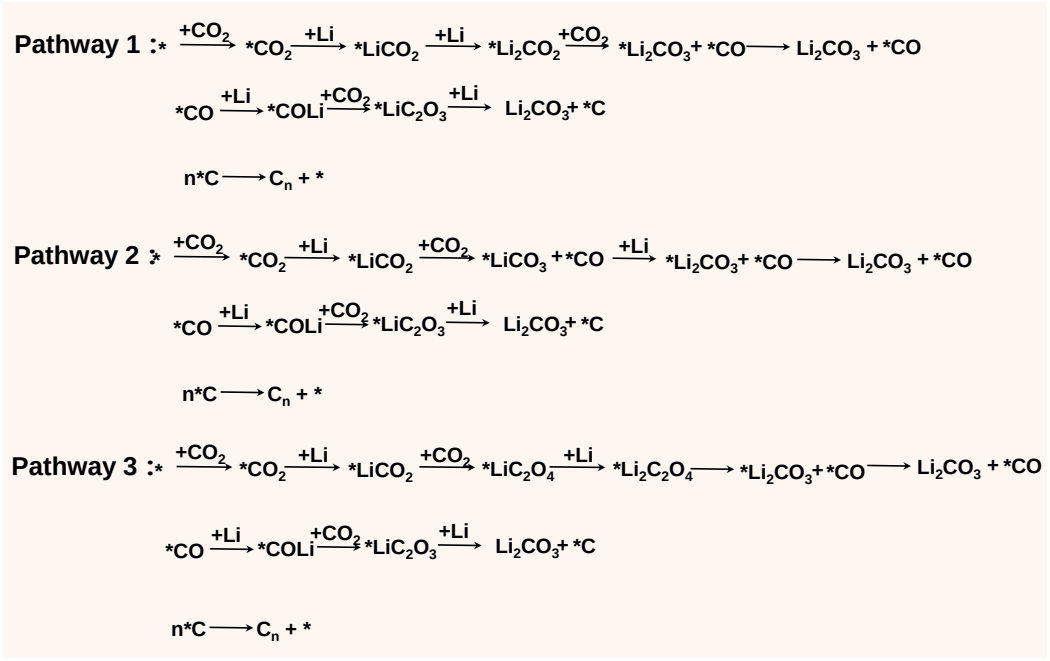

Figure S26. Possible discharge pathways at TAPP-Mn sites. The asterisk (*) represents the active metal sites for adsorption and reaction.

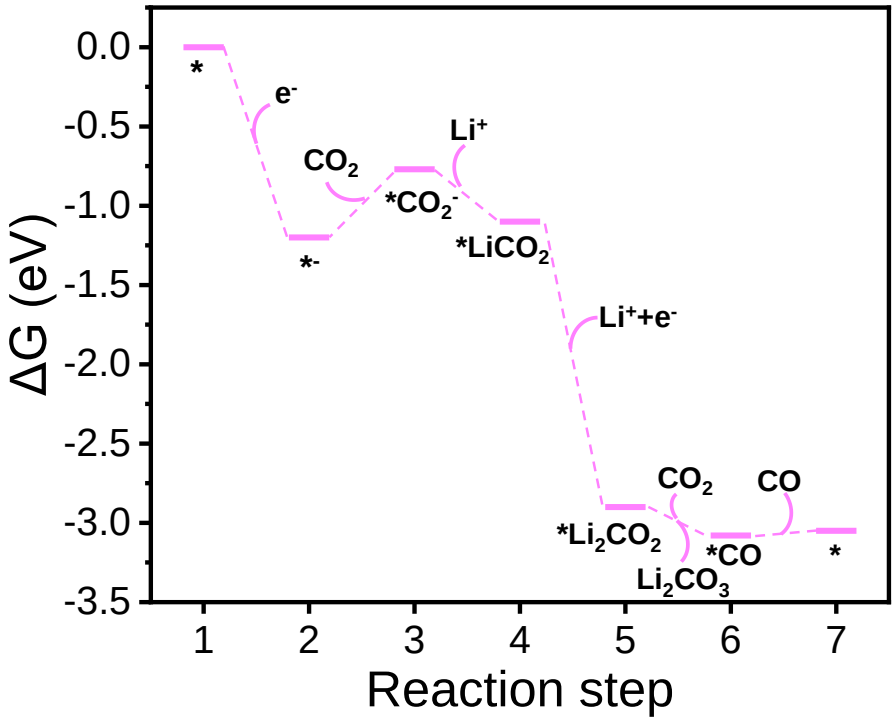

Figure S27. Calculated energetic profiles of Li_2CO_3 nucleation and CO formation on TAPP-Co molecule at U = 0 V.

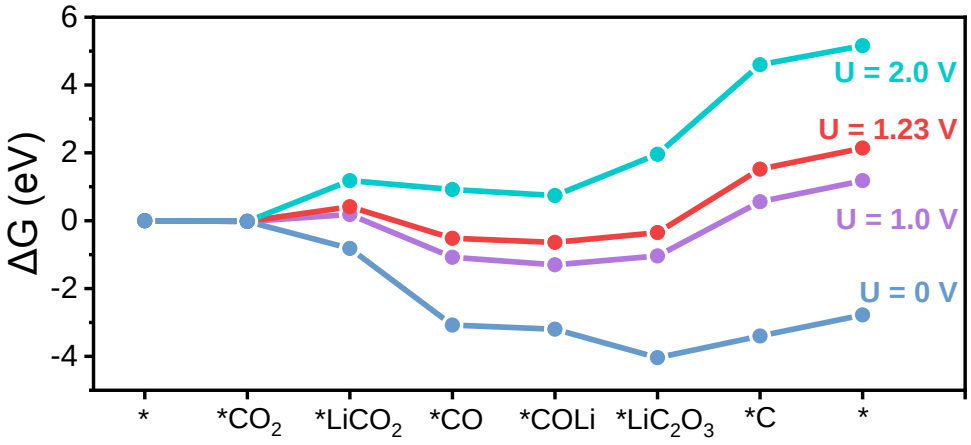

Figure S28. Calculated energetic profiles of the optimal discharge pathway at TAPP-Mn molecule at U = 0 V, 1.0 V, 1.23 V and 2.0 V.

Equation S2-S7

$$\mathbf{TAPP\text{-}Mn^{II} + e^- + Li^+ + CO_2 \rightarrow TAPP\text{-}Mn\text{-}CO_2Li} \quad \mathbf{\Delta G^0 = -0.82\ eV} \quad \mathbf{(Equation\ S2)}$$

$$\mathbf{TAPP\text{-}Co^{II} + e^- + Li^+ + CO_2 \rightarrow TAPP\text{-}Co\text{-}CO_2Li} \quad \mathbf{\Delta G^0 = -1.11\ eV} \quad \mathbf{(Equation\ S3)}$$

$$\mathbf{TAPP\text{-}Mn^{II} + e^- \rightarrow TAPP\text{-}Mn^{I}} \quad \mathbf{\Delta G^0 = -0.75\ eV} \quad \mathbf{(Equation\ S4)}$$

$$\mathbf{TAPP\text{-}Co^{II} + e^- \rightarrow TAPP\text{-}Co^{I}} \quad \mathbf{\Delta G^0 = -1.20\ eV} \quad \mathbf{(Equation\ S5)}$$

$$\mathbf{TAPP\text{-}Ni^{II} + e^- \rightarrow TAPP\text{-}Ni^{I}} \quad \mathbf{\Delta G^0 = -1.41\ eV} \quad \mathbf{(Equation\ S6)}$$

$$\mathbf{TAPP\text{-}Cu^{II} + e^- \rightarrow TAPP\text{-}Cu^{I}} \quad \mathbf{\Delta G^0 = -1.35\ eV} \quad \mathbf{(Equation\ S7)}$$

Table S2. The Li-CO_2 battery performance of some reported cathode catalysts including carbon-based materials, crystalline-based materials, COF-based materials, and Mn-based materials.

Cathode catalyst	Overpotential of 1st cycle	Discharge capacity (current density)	Cycle performance (current density, cut-off condition)	Ref.
TTCOF-Mn	**1.07 V (100 mA/g)**	**13018 mAh/g (100 mA/g)**	**180 cycles (300 mA/g, limited capacity of 1000 mAh/g)**	**This work**
COF-Ru@CNT	1.24 V (200 mA/g)	27348 mAh/g (200 mA/g)	200 cycles (200 mA/g, limited capacity of 1000 mAh/g)	9
Graphene	1.55 V (100 mA/g)	14722 mAh/g (50 mA/g)	20 cycles (50 mA/g, limited capacity of 1000 mAh/g)	10
BN-hG	1.1 V (100 mA/g)	16033 mAh/g (0.3 A/g)	200 cycles (1 A/g, limited capacity of 1000 mAh/g)	11
CQD/hG	1.02 V (100 mA/g)	12300 mAh/g (0.5 A/g)	235 cycles (1 A/g, limited capacity of 500 mAh/g)	12
CNT	1.65 V (50 mA/g)	5139 mAh/g (100 mA/g)	60 cycles (100 mA/g, limited capacity of 1000 mAh/g)	13
Mn_2(dobdc)	1.40 V (50 mA/g)	18022 mAh/g (50 mA/g)	50 cycles (200 mA/g, limited capacity of 1000 mAh/g)	14
CoPPc	1.50 V (0.05 mA/cm^2)	13.6 mAh/cm^2 (0.1 mA/cm^2)	50 cycles (0.05 mA/cm^2, limited capacity of 1 mAh/cm^2)	15
graphene@COF	1.08 V (500 mA/g)	27833 mAh/g (75 mA/g)	56 cycles (0.5 A/g, limited capacity of 1000 mAh/g)	16
P-Mn_2O_3/KB	1.40 V (50 mA/g)	9434 mAh/g (50 mA/g)	50 cycles (50 mA/g, limited capacity of 1000 mAh/g)	17
MnO@NC-G	1.18 V (100 mA/g)	25021 mAh/g (50 mA/g)	206 cycles (1000 mA/g, limited capacity of 1000 mAh/g)	18

References

1. Jin, S.; Sakurai, T.; Kowalczyk, T.; Dalapati, S.; Xu, F.; Wei, H.; Chen, X.; Gao, J.; Seki, S.; Irle, S.; Jiang, D., Two-Dimensional Tetrathiafulvalene Covalent Organic Frameworks: Towards Latticed Conductive Organic Salts. *Chem. Eur. J.* **2014,** *20* (45), 14608-14613.
2. Mitamura, Y.; Yorimitsu, H.; Oshima, K.; Osuka, A., Straightforward Access to Aryl-substituted Tetrathiafulvalenes by Palladium-Catalysed Direct C-H Arylation and Their Photophysical and Electrochemical Properties. *Chem. Sci.* **2011,** *2* (10), 2017-2021.
3. Lin, S.; Diercks, C. S.; Zhang, Y.-B.; Kornienko, N.; Nichols, E. M.; Zhao, Y.; Paris, A. R.; Kim, D.; Yang, P.; Yaghi, O. M.; Chang, C. J., Covalent Organic Frameworks Comprising Cobalt Porphyrins for Catalytic CO_2 Reduction in Water. *Science* **2015,** *349* (6253), 1208-1213.
4. Lu, M.; Liu, J.; Li, Q.; Zhang, M.; Liu, M.; Wang, J.-L.; Yuan, D.-Q.; Lan, Y.-Q., Rational Design of Crystalline Covalent Organic Frameworks for Efficient CO_2 Photoreduction with H_2O. *Angew. Chem. Int. Ed.* **2019,** *58* (36), 12392-12397.
5. Zhu, H.-J.; Lu, M.; Wang, Y.-R.; Yao, S.-J.; Zhang, M.; Kan, Y.-H.; Liu, J.; Chen, Y.; Li, S.-L.; Lan, Y.-Q., Efficient Electron Transmission in Covalent Organic Framework Nanosheets for Highly Active Electrocatalytic Carbon Dioxide Reduction. *Nat. Commun.* **2020,** *11* (1), 497.
6. Zhao, Y.; Truhlar, D. G., The M06 Suite of Density Functionals for Main Group Thermochemistry, Thermochemical Kinetics, Noncovalent Interactions, Excited States, and Transition Elements: Two New Functionals and Systematic Testing of Four M06-class Functionals and 12 Other Functionals. *Theor. Chem. Acc.* **2008,** *120* (1-3), 215-241.
7. Andrae, D.; Häußermann, U.; Dolg, M.; Stoll, H.; Preuß, H., Energy-adjusted*ab initio* Pseudopotentials for the Second and Third Row Transition Elements: Molecular Test for M_2 (M = Ag, Au) and MH (M = Ru, Os). *Theor. Chim. Acta* **1991,** *78* (4), 247-266.
8. Frisch, M. J., et al. Gaussian 09, Revision A.01, Gaussian, Inc., Wallingford CT, **2013**.
9. Li, X.; Wang, H.; Chen, Z.; Xu, H.-S.; Yu, W.; Liu, C.; Wang, X.; Zhang, K.; Xie, K.; Loh, K. P., Covalent-Organic-Framework-Based Li-CO_2 Batteries. *Adv. Mater.* **2019,** *31* (48), 1905879.
10. Zhang, Z.; Zhang, Q.; Chen, Y.; Bao, J.; Zhou, X.; Xie, Z.; Wei, J.; Zhou, Z., The First Introduction of Graphene to Rechargeable Li-CO_2 Batteries. *Angew. Chem. Int. Ed.* **2015,** *54* (22), 6550-6553.
11. Qie, L.; Lin, Y.; Connell, J. W.; Xu, J.; Dai, L., Highly Rechargeable Lithium-CO_2 Batteries with a Boron- and Nitrogen-Codoped Holey-Graphene Cathode. *Angew. Chem. Int. Ed.* **2017,** *56* (24), 6970-6974.
12. Jin, Y.; Hu, C.; Dai, Q.; Xiao, Y.; Lin, Y.; Connell, J. W.; Chen, F.; Dai, L., High-Performance Li-CO2 Batteries Based on Metal-Free Carbon Quantum Dot/Holey Graphene Composite Catalysts. *Adv. Funct. Mater.* **2018,** *28* (47),

1804630.
13. Li, C.; Guo, Z.; Yang, B.; Liu, Y.; Wang, Y.; Xia, Y., A Rechargeable Li-CO_2 Battery with a Gel Polymer Electrolyte. *Angew. Chem. Int. Ed.* **2017,** *56* (31), 9126-9130.
14. Li, S.; Dong, Y.; Zhou, J.; Liu, Y.; Wang, J.; Gao, X.; Han, Y.; Qi, P.; Wang, B., Carbon Dioxide in the Cage: Manganese Metal-Organic Frameworks for High Performance CO_2 Electrodes in Li-CO_2 Batteries. *Energy Environ. Sci.* **2018,** *11* (5), 1318-1325.
15. Chen, U.; Zou, K.; Ding, P.; Deng, J.; Zha, C.; Hu, Y.; Zhao, X.; Wu, D.; Fan, J.; Li, Y., Conjugated Cobalt Polyphthalocyanine as the Elastic and Reprocessable Catalyst for Flexible Li-CO_2 Batteries. *Adv. Mater.* **2019,** *31* (2), 1805484.
16. Huang, S.; Chen, D.; Meng, C.; Wang, S.; Ren, S.; Han, D.; Xiao, M.; Sun, L.; Meng, Y., CO_2 Nanoenrichment and Nanoconfinement in Cage of Imine Covalent Organic Frameworks for High-Performance CO_2 Cathodes in Li-CO_2 Batteries. *Small* **2019,** *15* (49), 1904830.
17. Ma, W.; Lu, S.; Lei, X.; Liu, X.; Ding, Y., Porous Mn_2O_3 cathode for highly durable Li-CO_2 batteries. *J. Mater. Chem. A* **2018,** *6* (42), 20829-20835.
18. Li, S.; Liu, Y.; Zhou, J.; Hong, S.; Dong, Y.; Wang, J.; Gao, X.; Oi, P.; Han, Y.; Wang, B., Monodispersed MnO Nanoparticles in Graphene-an Interconnected N-doped 3D Carbon Framework as a Highly Efficient Gas Cathode in Li-CO_2 Batteries. *Energy Environ. Sci.* **2019,** *12* (3), 1046-1054.